

Supporting Information

Experimental

Materials and Instrumentation

Gold(I) chloride (AuCl, 99.9%, Sigma-Aldrich), sodium citrate dihydrate ($C_6H_5Na_3O_7 \cdot 2H_2O$, $\geq 99.0\%$, Sigma-Aldrich), polyvinylpyrrolidone (PVP, Mw 10,000 $g \cdot mol^{-1}$, Sigma-Aldrich), sodium borohydride ($NaBH_4$, $\geq 98\%$, Sigma-Aldrich), hydroquinone ($C_6H_6O_2$, $\geq 99\%$, Sigma-Aldrich), L-ascorbic acid ($C_6H_8O_6$, $\geq 99.0\%$, Sigma-Aldrich) and hexadecyltrimethylammonium bromide (CTAB, $\geq 99\%$, Sigma-Aldrich) methanol (absolute grade - Synth – Brazil), ethanol (95 %, Synth – Brazil), and isopropanol (99.5 %, Sigma-Aldrich) were used as received. Deionized water was used throughout the experiments.

Instrumentation

Transmission and high-resolution transmission electron microscopy (TEM and HRTEM) images were taken on a JEOL JEM 2100 electron microscope operating at an accelerating voltage of 200 kV. The solid samples were dispersed in the appropriate solvent for 30 min under magnetic stirring, washed-centrifuged three times prior to the deposition on TEM grids (Formvar/Carbon Film coated, 200 Mesh, Cu). UV-vis diffusive reflectance spectra (DRS) were recorded on a Shimadzu UV-2600 spectrophotometer equipped with an integrating sphere (ISR 2600) using $BaSO_4$ as the reflectance standard sample. Powder X-ray diffraction (XRD) patterns were recorded in Shimadzu 7000 Maxima diffractometer with Cu $K\alpha$ radiation ($\lambda_{CuK\alpha} = 1.5418 \text{ \AA}$ for combined $K\alpha_1$ and $K\alpha_2$) in a Bragg-Brentano geometry. Each spectrum and diffractogram correspond to independent runs. X-ray Absorption spectroscopy (XAS) was used to follow the oxidation state of gold in function of the time of milling process. The X-ray Absorption Near Edge Spectroscopy (XANES) at Au L3 edge were recorded at Brazilian Synchrotron Light Laboratory (LNLS, UVX source) at XAFS2 beamline.¹ The beamline has a double-crystal Si 111 monochromator and ionization chambers as detectors. Spectra were acquired in transmission mode. Samples were deposited on and covered by Kapton® tapes and measured at room temperature. Data processing was performed with Demeter package.²

The milling procedure was stopped periodically, the sample was collected and immediately analyzed. In order to avoid major perturbations in the system, each withdrawal represented less than 3 % of the total amount of powder.

Mechano-colloidal synthesis of Au nanotadpoles

Step 1 – Ball milling step. In a typical 100 mg synthesis procedure, AuCl (16.4 mg, 0.07 mmol), sodium citrate (21.1 mg, 0.07 mmol), and PVP (62.5 mg, 0.56 mmol - with respect of the monomer unit) were milled in a PTFE milling jar of 14 mL using three ZrO₂ balls (10 mm, 3.17 g each) giving a ball-to-powder mass ratio (bpr) of 95:1 (for bpr = 190:1, six milling balls were employed). The milling device consists of a vibratory ball mill with fixed vibration frequency of 27.5 Hz (SL-38, SOLAB – Brazil). After milling for the specified time, the samples were recovered for direct analysis (UV-VIS DRS, XRD and XAS) and a part of it dispersed in water for TEM.

Step 2 – Solution phase step. Part of the milled solid sample was then dispersed in water (2 mg.mL⁻¹). After 30 min, *i.e.*, when no further color change was observed, the nanoparticles were isolated from the reaction mixture by centrifugation and re-dispersed in water. The solid sample was washed 3 times with water by successive cycles of centrifugation and removal of the supernatant, being finally re-dispersed in water for further use. Control experiments were performed in the same conditions as above by the changing the reductant (replacing sodium citrate by NaBH₄, hydroquinone, ascorbic acid or PVP), the capping agent (replacing PVP for CTAB), and the solvent (methanol, ethanol or isopropanol).

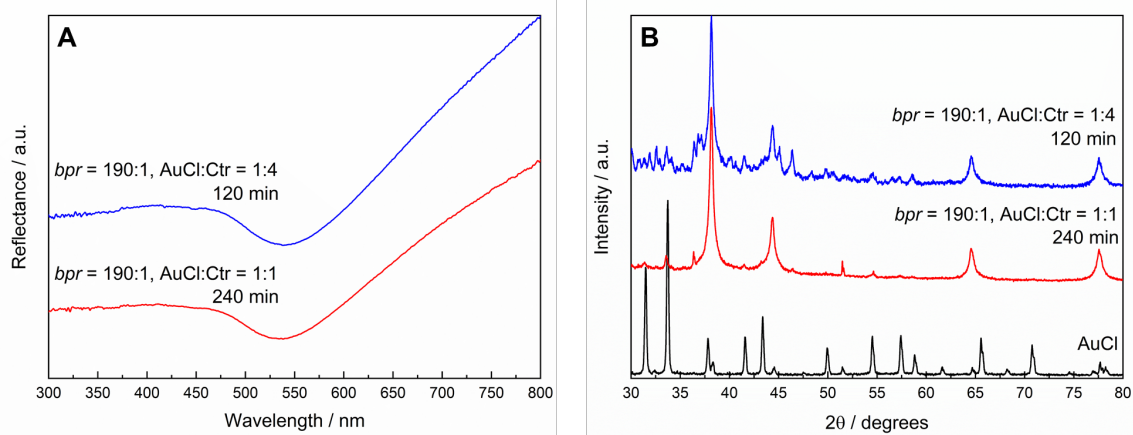


Figure S1. UV-VIS diffusive reflectance spectra (A) and XRD patterns (B) of the solid samples containing a mixture of AuCl, citrate, and PVP as a function of time during ball-milling. The *bpr* corresponded to 190:1. The Au:PVP molar ratio was kept at 1:8 while the Au:citrate corresponded to 1:1 or 1:4. Ball milling time corresponded to 120 or 240 min. The XRD pattern for AuCl is also shown for comparison. Under these conditions, the signals assigned to the presence of AuCl precursor are much more less intense as compared to Figure 2.

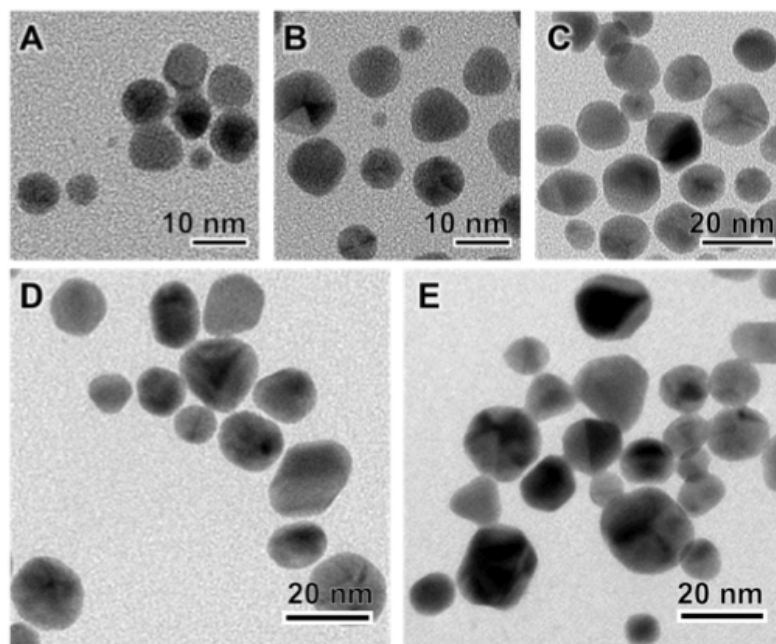


Figure S2. TEM images for the nanomaterials produced by employing 30 (A), 60 (B), 120 (C), 240 (D), and 360 (E) min as the ball-milling followed by dispersion in isopropanol to avoid the morphological evolution to tadpoles (*bpr* 95:1; Au:citrate and Au:PVP molar ratios corresponding to 1:1 and 1:8, respectively). The formation of only spherical particles were detected, which increase in size with the ball milling time.

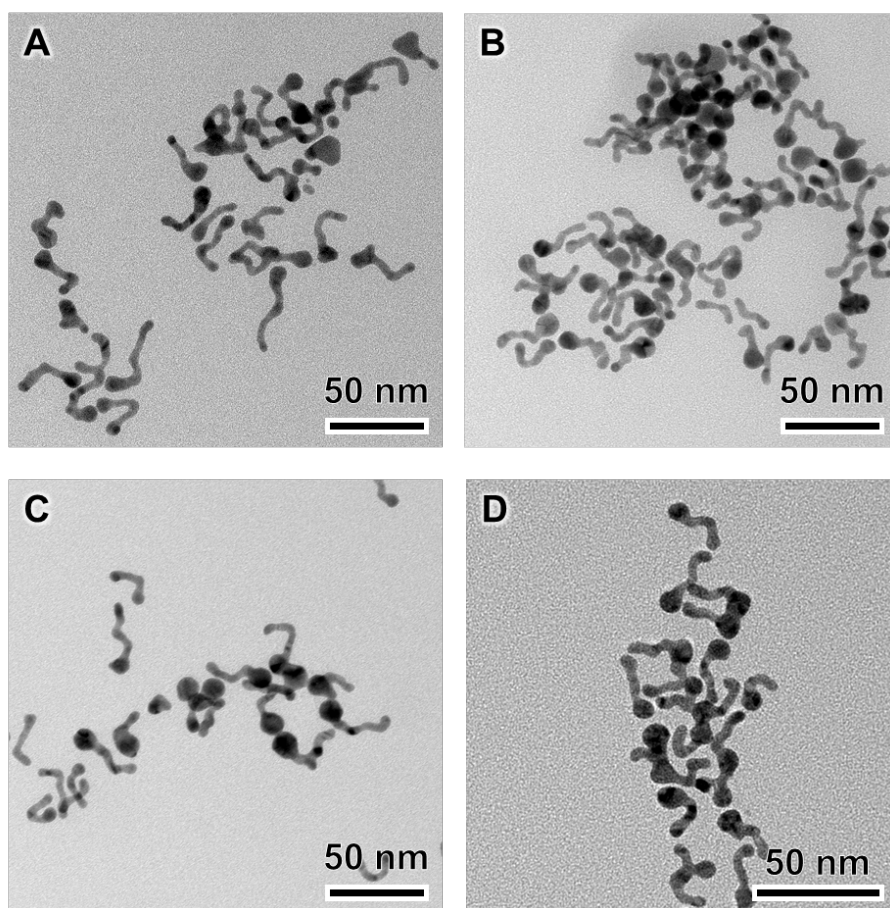


Figure S3. TEM images for the nanomaterials produced by employing 30 (A), 60 (B), 90 (C), and 240 (D) min as the ball-milling followed by dispersion in water for 30 min (*bpr* 95:1; Au:citrate and Au:PVP molar ratios corresponding to 1:1 and 1:8, respectively). The formation of the nanotadpoles was detected in all cases due to the presence of both Au NPs and AuCl in the solid reaction mixture after the ball-milling step.

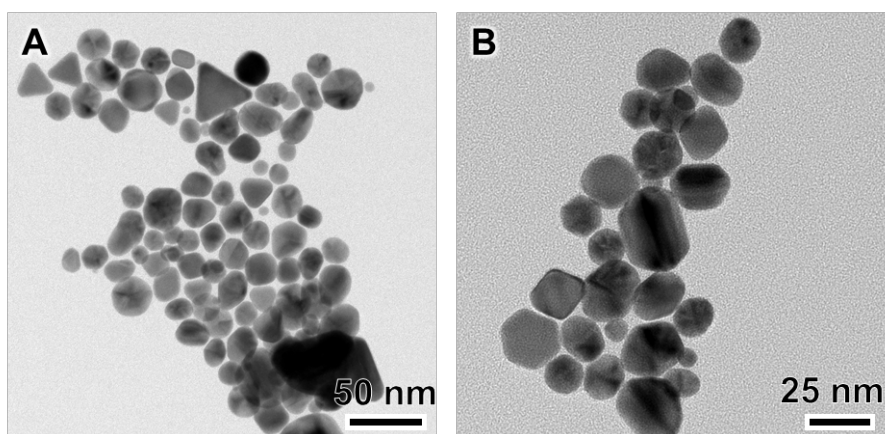


Figure S4. TEM images for the nanomaterials produced by employing 120 min as the ball-milling time followed by dispersion in water for 30 min. Here, the *bpr* was increased to 190:1 (Au:citrate and Au:PVP molar ratios corresponding to 1:4 and 1:8, respectively). The formation of nanotadpoles was not observed as most of the AuCl precursor is consumed during the ball-milling step under *bpr* 190:1 and higher citrate concentration.

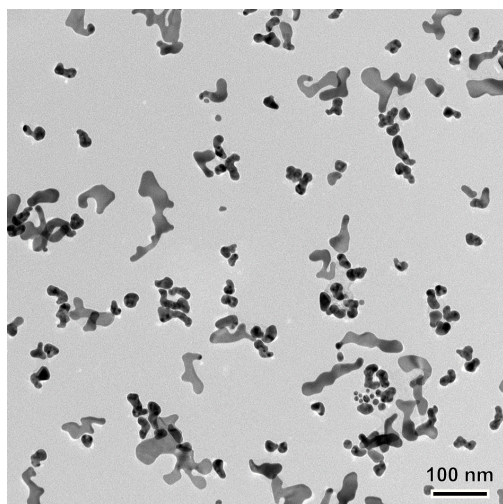


Figure S5. TEM micrograph of Au nanostructures that were obtained by employing a solid mixture containing AuCl, citrate, and PVP as the starting materials for a water solution-phase step (without the previous ball-milling step). These samples were obtained after 12 days in solution.

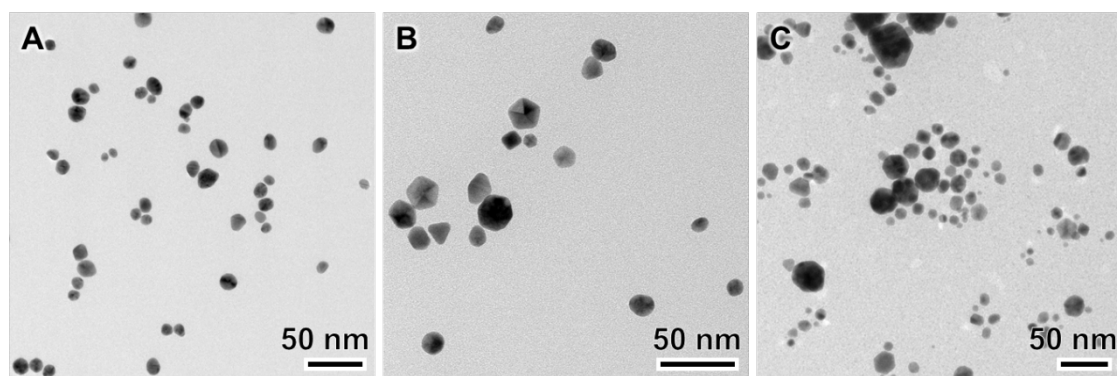


Figure S6. TEM images for the samples obtained by the mechano-colloidal approach under the same conditions as described in Figure 2 by replacing water as the solvent by (A) MeOH, (B) EtOH and (C) *i*-PrOH. Nanotadpoles were not formed under these conditions.

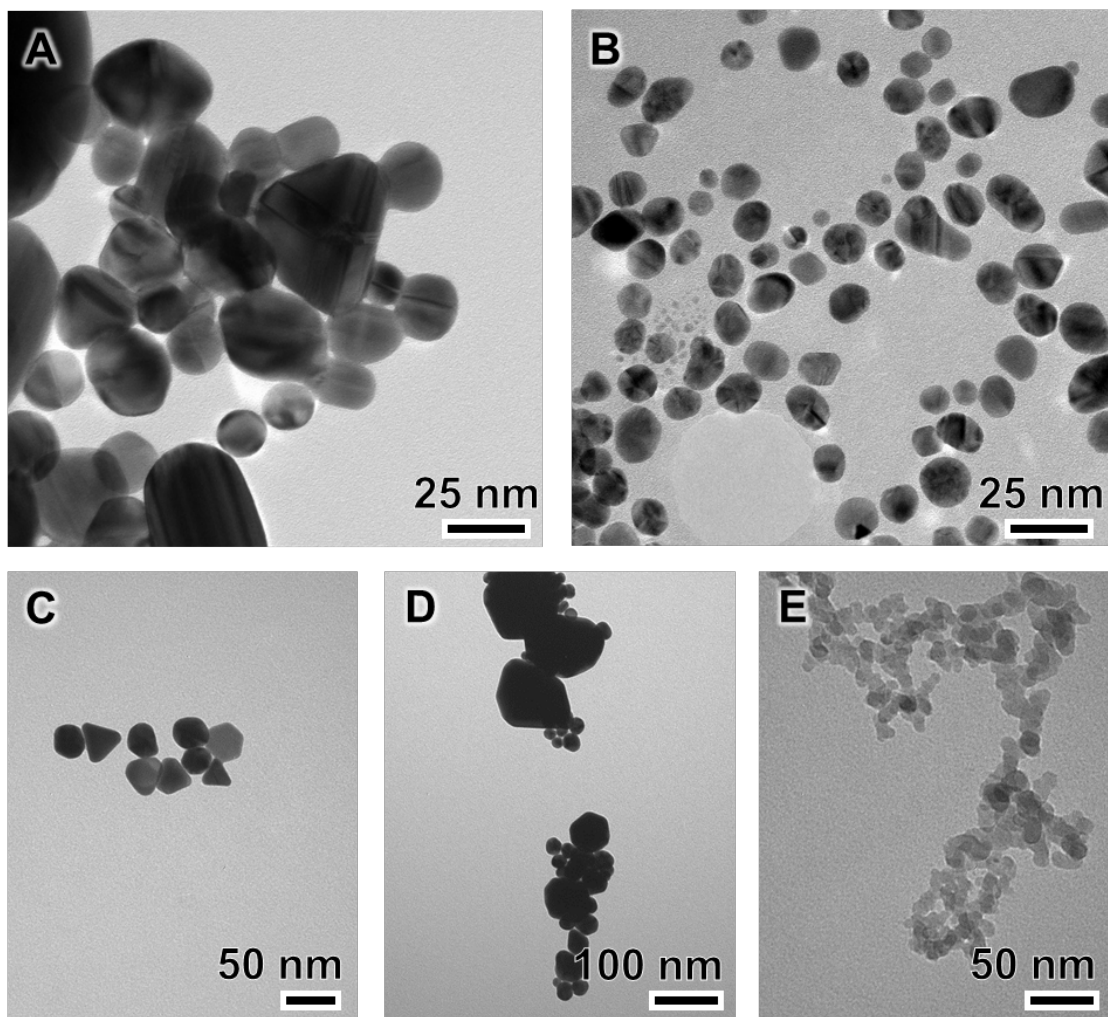


Figure S7. Control experiments varying the nature of the reducing and capping agent in the mechano-colloidal synthesis: (A-B) NaBH_4 as reductant and CTAB (A) and PVP (B) as capping agents. (C-E) PVP as capping agent and ascorbic acid (C), PVP only (D) and hydroquinone (E) as reductants.

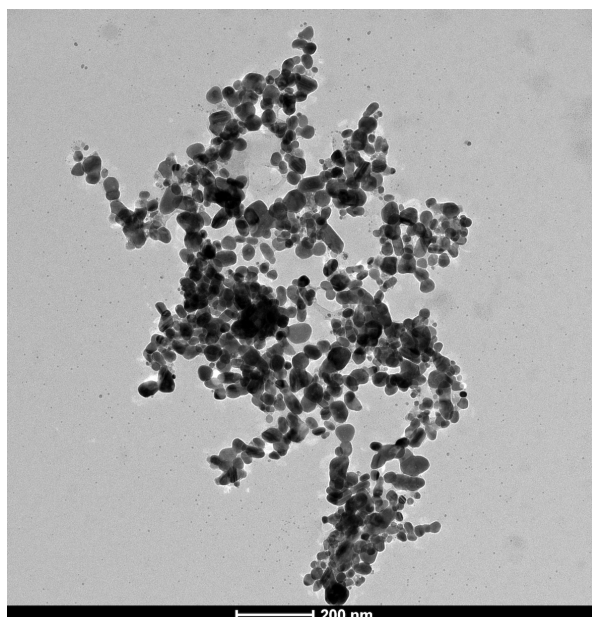


Figure S8. Mechano-colloidal approach to the synthesis of Ag NPs under similar conditions as described for Au NPs. In this case, although some Ag NPs with elongated shapes could be detected, the formation of uniform and well-defined tadpoles was not detected (Fig. S8). This observation suggests that the application of the mechano-colloidal approach to other metal NPs requires further optimizations in terms of the choice of reducing and stabilizing agents to enable shape control.

1. S. J. A. Figueroa, J. C. Mauricio, J. Murari, D. B. Beniz, J. R. Piton, H. H. Slepicka, M. F. De Sousa, A. M. Espíndola and A. P. S. Levinsky, 2016, **712**, 012022.
2. B. Ravel and M. Newville, *Journal of Synchrotron Radiation*, 2005, **12**, 537-541.